Clinical & Experimental Metastasis (2025) 42:10
https://doi.org/10.1007/s10585-024-10323-0

RESEARCH ARTICLE

m1A-regulated DIAPH3 promotes the invasiveness of colorectal cancer via stabilization of KRT19

Shuyi Mi[1,2] · Jie Hu[1,3] · Wenwen Chen[1,2] · Jingyu Chen[1,2] · Zhipeng Xu[1] · Meng Xue[1,2]

Received: 12 June 2024 / Accepted: 4 October 2024

Abstract

Background In recent years, the emphasis has shifted to understanding the role of N1-methyladenosine (m1A) in tumor progression as little is known about its regulatory effect on mRNA and its role in the metastasis of colorectal cancer (CRC).

Methods We performed methylated RNA immunoprecipitation sequencing of tumor tissues and tumor-adjacent normal tissues from three patients with CRC to determine the m1A profile of mRNA in CRC. The expression of diaphanous-related formin 3 (DIAPH3) and its correlation with clinicopathological characteristics of CRC were evaluated using immunohistochemistry and online datasets. The role of DIAPH3 in the migration and invasion of CRC cells was evaluated using wound healing assay, Transwell assay and xenograft metastatic model. The downstream targets of DIAPH3 were screened using mass spectrometry. By co-transfecting DIAPH3 siRNA and a keratin 19 (KRT19) ectopic plasmid into CRC cells, the role of DIAPH3-KRT19 signaling axis was confirmed.

Results The mRNA level of DIAPH3 and its m1A modifications increased simultaneously in the CRC tissues. In addition, high DIAPH3 expression in CRC tissues is significantly associated with metastasis and progression to an advanced stage. After the knockdown of DIAPH3, the migration and invasion capabilities of CRC cells suffered a notable decline, which could be rescued by overexpressing KRT19. In addition, the proteasome inhibitor MG132 could block the degradation of KRT19 induced by DIAPH3 silencing.

Conclusions Our study reveals that DIAPH3 mRNA was modified in CRC cells by m1A methylation. Silencing DIAPH3 suppresses the migration and invasion of CRC cells, potentially through the proteasome-dependent degradation of downstream KRT19.

Keywords CRC · m1A · DIAPH3 · Migration · Invasion

Abbreviations

AJCC	American Joint Committee on Cancer
CHX	Cycloheximide
COAD	Colon adenocarcinoma
CRC	Colorectal cancer
DIAPH3	Diaphanous-related formin 3
GEO	Gene Expression Omnibus
GEPIA	Gene Expression Profiling Interactive Analysis
FBS	Fetal bovine serum
KO	Knockout
KRT19	Keratin 19
IHC	Immunohistochemistry
LncRNA	Long non-coding RNA
3-MA	3-Methyladenine
m1A	N1-methyladenosine
m6A	N6-methyladenosine
MeRIP-seq	Methylated RNA immunoprecipitation sequencing
MFAP2	Microfibril associated protein 2
MS	Mass Spectrometry
READ	Rectal adenocarcinoma

Shuyi Mi and Jie Hu have equally contributed to this work.

✉ Zhipeng Xu
2311036@zju.edu.cn

✉ Meng Xue
xuemeng@zju.edu.cn

[1] Department of Gastroenterology, The Second Affiliated Hospital of Zhejiang University School of Medicine, No.88, Jiefang Road, Hangzhou 310009, Zhejiang, China

[2] Institute of Gastroenterology, Zhejiang University, Hangzhou, China

[3] Department of Gastroenterology, Jiande First People's Hospital, Jiande, Hangzhou, China

Published online: 22 January 2025

qPCR	Quantitative real-time PCR
RIP	RNA immunoprecipitation
TCGA	The Cancer Genome Atlas

Introduction

The significance of genomic, epigenomic, and transcriptomic regulation across the entire cancer life cycle has been extensively studied [1]. Recently, a type of post-transcriptional modifications occurring on RNA molecules called "epitranscriptomics" has gained attention. This includes processes such as RNA editing, slicing and methylation [2]. Among these modifications, RNA methylation, especially N6-methyladenosine (m6A), has been well studied and is considered to play a vital role in the development of various cancers [3]. In recent years, another modification, N1-methyladenosine (m1A), has gained attention [4]. In addition to an added methyl group, m1A also endows modified adenosine with a positive charge, which may have a stronger effect on the RNA sequence structure and protein-RNA interactions than m6A, although the abundance of m1A is much lower than that of m6A [5].

Accumulating evidence has demonstrated that m1A plays a significant regulatory role in various cancers [6–8]. Colorectal cancer (CRC) is a common malignancy globally [9]. For metastatic CRC, the 5-year overall survival rate is only 4–12% [10]. In our previous study, the profile of m1A modifications in long noncoding RNA (lncRNAs) and several m1A-modified lncRNAs were thought to be associated with CRC prognosis [11]. In addition, m1A demethylase alkB homology 1 (ALKBH1) was found to affect CRC metastasis [12]. We performed methylated RNA immunoprecipitation sequencing (MeRIP-seq) to explore differentially methylated peaks within mRNAs by comparing CRC samples and tumor-adjacent normal tissues, and identified differentially expressed mRNAs simultaneously. Microfibril-associated protein 2 (MFAP2), whose mRNA is overexpressed and m1Ahypermethylated in CRC, was found to promote CRC invasion in our recent study [13].

In this study, we identified Diaphanous-related formin 3 (DIAPH3), a member of formin family of cytoskeletal regulators, has increased level of both mRNA expression and m1A level. Moreover, we demonstrated that DIAPH3 plays a pivotal part in the migration and invasion of CRC cells, representing an alternative target for individual treatment strategies.

Materials and methods

Clinical CRC samples

Ethcs approval was obtained from the Human Research Ethics Committee of the Second Affiliated Hospital School of Medicine, Zhejiang University (Approval number: 20220034). All samples were obtained from CRC patients undergoing surgical resections at the Second Affiliated Hospital, School of Medicine, Zhejiang University with written consent forms. For m1A MeRIP sequencing, three pairs of tumor and adjacent non-tumorous tissues were used. For m1A methylation assay of DIAPH3 mRNA, RNAs from tumor and adjacent non-tumorous tissues of 24 CRC patients were collected. For immunohistochemistry (IHC), 177 pairs of paraffin-embedded tissues, including three cohorts (cohort 1:90 pairs; cohort 2:30 pairs; and cohort 3:57 pairs), were collected from the archive cabinet of the pathology department. Accordingly, three tissue arrays were prepared in cooperation with Outdo Biotechnology (Shanghai, China).

A supplementary illustration for all the samples that were used in each experiment was listed in Supplementary Table S1.

IHC

Paraffin-embedded tissue samples were deparaffinized in 100% xylene and rehydrated through a graded series of ethanol concentrations. The slides were then heated in citrate buffer (pH 6.0) at 95 °C for 5 min for antigen retrieval. Endogenous peroxidase was blocked with 3% H_2O_2. Then these tissue samples were naturally cooled to room temperature. Sections were then conjugated with DIAPH3 antibody at 4 °C overnight and then incubated with HRP-conjugated secondary antibody for 30 min. After washing the slides three times with PBS, the color was developed using the DAB Chromogen. The slides were then rinsed with tap water and counterstained with hematoxylin. Five random fields per section were viewed under a light microscope (Leika, Wetzler, Germany), and the expression of DIAPH3 was scored in terms of the intensity of staining and the percentage of positively stained cells. The proportion of positive cells in each specimen was quantified under a microscope and the cells were classified into four groups. 0:0–5% positive cells; 1:6–50% positive cells; 2:51–75% positive cells; 3:76–100% positive cells. The intensity of DIAPH3 staining was graded as follows: 0, no staining; 1, weak staining; 2, moderate staining; 3, dense staining (Supplementary Fig. S1). Multiplying the score of the intensity by the proportion of positive staining was defined as the DIAPH3 staining score.

Cell culture and treatment

Two human CRC cell lines, HCT116 and RKO, were purchased from the American Type Culture Collection and cultured in McCoy's 5A and EMEM medium, respectively. The medium was supplemented with 10% fetal bovine serum (FBS; ExCell Bio, Taicang, China) at a 37 °C atmosphere of 5% CO2.

Cells were plated in a 6-well dish 18 h before transfection. Lipofectamine 3000 (Invitrogen, Carlsbad, CA, USA) was used to deliver plasmids into CRC cells according to the manufacturer's instructions. siRNAs targeting human DIAPH3 (Tsingke Biotechnology Company, Beijing, China) were transfected with Lipofectamine RNAiMAX transfection reagent (Invitrogen, Carlsbad, CA, USA) in Opti-MEM (Gibco, California, USA). The siRNAs sequences were: si-DIAPH3-1, sense 5'-GAGUGAAUAUAGCAACUUATT-3′; si-DIAPH3-2, sense 5′-GAGUGAAUAUAGCAACUU ATT-3′; si-TRMT6, sense 5'-AGAUCGAAGUCAUCCUAA ACU-3′.

For the protein stability assessment, CRC cell lines were incubated with cycloheximide (CHX, MedChemExpress, New Jersey, USA) at 100 mg/ml for different lengths of time. To figure out the protein degradation pathway, CRC cell lines were also incubated with proteasome inhibitor MG132 (20 μM, MedChemExpress) for 24 h or autophagy inhibitor 3-MA (2.5 mM, MedChemExpress) for 24 h.

Mining the database

We used the GEPIA2 website (http://gepia2.cancer-pku.cn/) to analyze DIAPH3 expression in colon adenocarcinoma (COAD) and rectum adenocarcinoma (READ). Correlation analysis between DIAPH3 and m1A regulators was performed using GEPIA. Survival analysis of DIAPH3 was performed using the online database GenomicScape (http://www.genomicscape.com/) [14]. The sample information and expression data are available in the Gene Expression Omnibus (GEO) database [Accession nos. GSE17538].

RNA extraction and quantitative real-time PCR (qPCR)

Total RNA was extracted from tissue samples and cells using TRIzol reagent (Invitrogen, Carlsbad, CA, USA) according to the manufacturer's instructions. One microgram of RNA per sample was reverse-transcribed to cDNA using HiScript II Q RT SuperMix for qPCR (Vazyme, Nanjing, China), and the latter was amplified using ChamQ Universal SYBR qPCR Master Mix (Vazyme). The relative expression of DIAPH3 was calculated by the 2-ΔΔCt method, with GAPDH as the internal control. The primer sequences are listed in Supplementary Table S2.

MeRIP-qPCR

For MeRIP-qPCR, One-tenth of the total RNAs was reserved as input. The remaining RNA was immunoprecipitated with m1A antibody (MBL, Tokyo, Japan) in RIP buffer (10 mM Tris HCl, 150 mM NaCl, 0.1% NP-40, and 0.2% RNase inhibitor) supplemented with RNase inhibitors for 2 h at 4 °C. Above mixtures were then added into Protein A/G beads (Invitrogen, California, USA), prewashed with RIP buffer, and rotated for an additional 2 h at 4 °C. After washing the sediment five times with RIP buffer, we eluted RNA from the beads. Then glycogen and isopropanol were added into the supernatant and incubated for 4 h at 4 °C. After the eluted RNA was washed with ethanol, the pellet was resuspended in RNase-free water for further use. Finally, the eluted and input RNAs were reverse-transcribed and analyzed using qPCR. The relative enrichment of m1A containing mRNA was calculated by normalization to the input.

MeRIP-seq and data analysis

MeRIP-seq was performed as described previously [11]. Total RNA (1 μg) was isolated from the tumor and adjacent normal tissues using Trizol (Invitrogen, Carlsbad, CA, USA) and sent to Cloud-Seq Biotech for m1A RNA immunoprecipitation (RIP) sequencing. After removing the rRNAs using Ribo-Zero rRNA Removal Kits (Illumina, California, USA) following the manufacturer's instructions, total RNA was subjected to immunoprecipitation with the GenSeqTM m1A-IP Kit (GenSeq Inc., China). RNA libraries were constructed by using rRNA-depleted RNAs with TruSeq Stranded Total RNA Library Prep Kit (Illumina) according to the manufacturer's instructions. Libraries were controlled for quality and quantified using the BioAnalyzer 2100 system (Agilent Technologies Inc., California, USA). 10 pM libraries were denatured as single-stranded DNA molecules, captured on Illumina flow cells, amplified in situ as clusters and finally sequenced for 150 cycles on Illumina NovaSeq Sequencer (Illumina).

The subsequent bioinformatics analysis was also done by Cloud-Seq Biotech. At first, paired-end reads were harvested from NovaSeq sequencer, then subjected to image analysis, base identification and quality control to make the data more reliable. Then, 3' adaptor and low-quality reads were identified and trimmed by cutadapt software (v1.9.3) [15]. Next the Hisat2 software (v2.0.4) were utilized to match clean reads for all samples to the reference genome (UCSC HG19) [16]. MACS software and diffRep software were then used to identify methylated genes in each sample and differential methylation sites respectively [17, 18]. The fragments per kilobase of exon per million fragments mapped (FPKM) value was obtained as the expression profiles of mRNA by Cuffdiff software (v2.2.1) [19]. Based on FPKM, fold change and p-value were calculated, differentially expressed mRNA were identified. Peaks with p value < 0.05 and q value < 0.1 were screened out. To screen for genes that were not rare, transcripts with FPKM > 10 in either CRC or adjacent normal tissues were selected. If more than one m1A peak was acquired for a single transcript, only the peak that changed the most was selected for further analysis.

Western blotting

Cells were lysed using radioimmunoprecipitation assay lysis buffer (Beyotime, Shanghai, China) supplemented with phenylmethanesulfonyl fluoride (Beyotime). Proteins were quantified using a BCA Protein Assay Kit (Fude Biological Technology, Hangzhou, China) and equal amounts per sample were separated by SDS-PAGE and transferred onto a PVDF membrane (Millipore). The membranes were blocked with 5% skim milk for 1 h at 25 °C, and then incubated overnight with primary antibodies against DIAPH3 (Proteintech, Wuhan, China), TRMT6 (Abclonal, Wuhan, China), BRD9 (Abclonal), keratin 19 (KRT19, Abclonal), SMYD3 (Abclonal), ARL2 (Abclonal), RIN1 (Abclonal), CAVIN3 (Abclonal), GGNBP2 (Absin, Shanghai, China), and GAPDH (Diagbio, Hangzhou, China) at 4 °C. After incubation for 1 h with an HRP-conjugated secondary antibody (Beyotime, Shanghai, China) at 25 °C, the membranes were washed three times with TBST, and the bands were visualized using an enhanced chemiluminescence reagent (NCM Biotech, Suzhou, China).

Scratch wound assay

The CRC cells were cultured in 24-well plates. After overnight incubation, we scratched the area in the middle of the well with a 10 μL pipette tip and washed the floating cells with PBS. At 0 and 24 h after wounding, images were captured using a light microscope (Leika, Wetzler, Germany). The width between the two boundary lines was measured using IMAGEJ software version 1.8.0.345 (NIH, Maryland, USA). Percentage of relative closure (%) = (width on day 0—width on day 24)/width on day 0 × 100.

Cell migration and invasion assays

The cell migration and invasion assays were performed using 24-well Transwell apparatus (8-μm pore size, Corning, NY, USA). A total of 8×10^4 cells per well were seeded in the uncoated upper chamber for cell migration assays, whereas 10×10^4 cells were seeded in Matrigel (Nova Pharmaceutical Technology, Shanghai, China)-coated chambers for cell invasion assays. The lower chambers were filled with a medium containing 20% FBS. After 48 h of incubation at 37 °C, the cells that had migrated from the upper to the lower surface of the filters were washed thrice with PBS, fixed in 4% paraformaldehyde for 15 min, stained with 0.05% crystal violet for 10 min at 25 °C, and washed twice with PBS. The cells were counted in five random fields (200 × magnification) per sample under a light microscope (Leika, Wetzler, Germany).

CRISPR/Cas9-driven gene knockout

The genomic deletion of DIAPH3 in colon cell lines (HCT116 and RKO) was carried out using CRISPR/Cas9 vector with a specific DIAPH3 guide RNA sequence (gRNA: 5′-CTCTGCGGTATGCATTGTAG-3′). After 48 h of transfection, single cells were sorted by FACS based on GFP expression in 96-well plates to obtain DIAPH3 knockout (KO) clones. Complete KO was confirmed by Sanger sequencing and western blotting using a DIAPH3 antibody.

Mass spectrometry (MS) analysis

After digesting the protein suspension overnight at 37 °C with trypsin (Beyotime, Shanghai, China), TMT reagent (Invitrogen, California, USA) was added to label the resulting peptides. The complexes were sent to LC Sciences (Hangzhou, China) for MS analysis, and reversed-phase chromatography was conducted to fractionate the TMT-labeled peptides. The fractionated peptide mixtures were loaded onto a C18-reversed phase analytical column and separated by mixing formic acid with acetonitrile. LC–MS/MS experiments were performed in positive ion mode on a Q Exactive Plus mass spectrometer (Invitrogen, California, USA). The MS data were obtained by selecting the most abundant precursor ions from the survey scans. The output files were processed using the MASCOT engine (Matrix Science, version 2.6) embedded in Proteome Discoverer 2.2. The tolerance for the precursor mass was 10 ppm, and that for the fragments was 0.05 Da. Proteins with a fold change > 1.3 and a p value < 0.1 were identified as differentially expressed proteins.

Xenograft metastatic model

All animal experiments were approved by the Animal Care and Use Committee of the Second Affiliated Hospital School of Medicine, Zhejiang University (Approval number: 2022002). Female BALB/c nude mice (aged 4 weeks) were purchased from the Institute for Experimental Animals of the Chinese Academy of Vital Rivers (Beijing, China). All the mice were housed in a specific pathogen-free environment at the Animal Facility of the Second Affiliated Hospital of Zhejiang University School of Medicine. After the DIAPH3 KO clone was obtained, cells were transfected with PGMLV-CMV-luc-PGK-neo. We injected 2×10^6 DIAPH3-KO or Negative-KO HCT116 cells into mice intraperitoneally (n = 5). After 28 days, the mice were intraperitoneally administered D-luciferin (1.5 mg) and imaged weekly using an IVIS (PerkinElmer IVIS Lumina XRMS Series III imaging system) to measure the luciferase signal intensity. Once a significant difference in luciferase signal intensity was observed between the two groups, the mice were sacrificed.

Statistical analysis

Each experiment was repeated at least thrice. Two groups were compared using a two-tailed unpaired Student's t test. Chi-square tests were used to analyze the significance of categorical data. Survival rates were calculated using the Kaplan–Meier method and compared using the log-rank test. Statistical analyses were performed using GraphPad Prism 8 software. Unless otherwise specified, $p < 0.05$ was considered statistically significant.

Results

m1A upregulated the expression of DIAPH3 in CRC cells

We first performed MeRIP-seq analysis of tumor tissues and tumor-adjacent normal tissues from three patients with CRC to delineate m1A methylation status and mRNA expression in CRC. When the alteration threshold was set at fivefold, more mRNAs showed a trend of expression levels consistent with the abundance of m1A modifications (Fig. 1A). Considering that the abundance of m1A in mRNA was relatively low [5], we selected 43 transcripts with both hyper-m1A-peaks and increased expression for further investigation. To explore novel metastasis-related genes in CRC, transcripts reported in other studies were excluded, and we focused on the remaining 12 genes (Supplementary Table S3). These 12 genes were measured using qPCR in the same three pairs of CRC tissues, and the expression of DIAPH3 increased the most in CRC (Fig. 1B). Also, the m1A-peak map obtained by visualization analysis of the sequencing showed increased m1A modifications in DIAPH3 mRNA in CRC (Fig. 1C). Furthermore, we performed MeRIP-qPCR analysis to evaluate the expression of DIAPH3 mRNA as well as its m1A methylation level on tumor tissues and its adjacent normal tissues from 24 CRC patients. The results showed that the expression of both DIAPH3 mRNA and $^{m1A+}$DIAPH3 mRNA were significantly higher in cancer tissues than those in matched adjacent normal tissues (Supplementary Fig. S2A, B).

It is known that the abundance of RNA post-transcriptional modifications depends on the activity of writer complexes and eraser proteins [20]. Because the m1A abundance of most mRNAs in CRC showed an upregulatory trend, we hypothesized that tumor-promoting methyltransferases or antineoplastic demethylases of m1A might regulate the m1A abundance of DIAPH3 mRNA. Based on Kaplan–Meier analysis of different m1A regulators with CRC prognosis in a previous study [21], we chose three potential m1A regulators for further study: TRMT61A, TRMT6, and ALKBH3. Based on the GEPIA database, we found that the correlation between TRMT6 and DIAPH3 expression was the most significant (Fig. 1D and Supplementary Fig. S3A, B). Therefore, TRMT6 was used as a tool to confirm m1A methylation status. After transfecting TRMT6 siRNA into HCT116 and RKO cells (Fig. 1E), the expression of DIAPH3 mRNA and $^{m1A+}$DIAPH3 mRNA was downregulated (Fig. 1F, G). Above results indicated that the m1A methylation modification may upregulate the mRNA expression of DIAPH3 in colorectal cancer cells.

The expression of DIAPH3 was upregulated and correlated with metastasis in CRC patients

According to the database GEPIA, we found that DIAPH3 expression was notably increased in CRC (Fig. 2A). After mining the GenomicScape database, further analysis showed that patients with high DIAPH3 in CRC tended to have shorter survival times than those with low expression (Fig. 2B).

To confirm the expression pattern of DIAPH3 in CRC tissues, we performed IHC staining on three tissue slides from 177 patients with CRC. When conducting the IHC assay, one point of tumor tissue and three points of adjacent normal tissue in cohort 1 were detached from the slides. Consequently, we compared the protein levels of DIAPH3 in 173 pairs of CRC tissues and adjacent non-cancerous tissues and conducted a correlation analysis between the expression of DIAPH3 in tumor tissues and clinicopathological characteristics using 176 CRC samples. It can be observed that in normal colorectal tissues, the staining is weaker than that in CRC tissues (Fig. 2C, D), which was consistent with the data-mining results described above. In addition, high protein level of DIAPH3 in CRC tissues was significantly associated with lymph node metastasis, and tended to develop more distant metastases, and progress to an advanced AJCC stage (Table 1). In the cohort of 89 patients with CRC with follow-up information, high DIAPH3 expression in tumor tissues was inversely correlated with the outcome (Fig. 2E). In order to recognize the involvement of DIAPH3 in the metastasis of CRC, the expression of DIAPH3 mRNA in tumor tissues from 24 CRC patients with or without metastasis were measured. It showed that the expression of DIAPH3 mRNA in CRC patients at M1 was higher than those patients at M0 (Supplementary Fig. S4A). Taken together, DIAPH3 was overexpressed in CRC, especially in patients with metastasis.

DIAPH3 regulates the migration and invasion of CRC cells

To determine the biological function of DIAPH3 in CRC, we knocked down DIAPH3 expression in HCT116 and RKO cells using two DIAPH3 siRNAs, and the

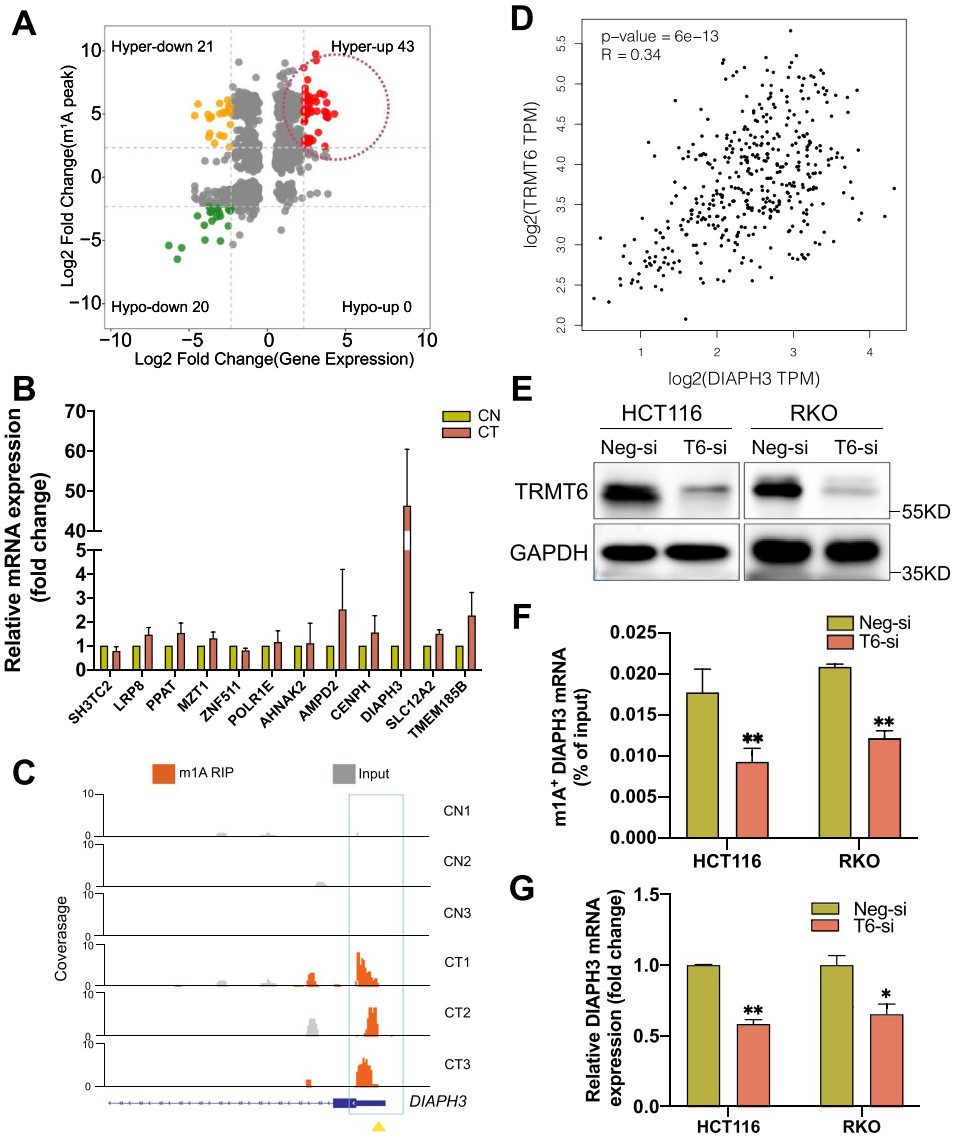

Fig. 1 m1A upregulated the expression of DIAPH3 in CRC cells. **A** The star plot shows the distribution of genes with both differential (hyper or hypo) m1A peaks and differential mRNA (up or down) expression (n = 3). The fold change of either expression or m1A methylation of mRNA < 5 is labeled as gray dots, while the others are marked with dots of different colors. The red dots highlighted by a circle represent up-regulated transcripts with an increased abundance of m1A in CRC tissues. **B** qPCR validation of the genes with the FPKM values increased most markedly in colorectal tumor (CT), when compared to adjacent normal tissues (CN) (n = 3). **C** A visualized m1A-peak map along the mRNA of DIAPH3 in colorectal tumor (CT) and adjacent normal tissues (CN). **D** A significant positive correlation (r = 0.34, p = 6e−13) was found between DIAPH3 mRNA and TRMT6 mRNA in CRC according to the GEPIA database. **E** The protein expression level of TRMT6 after transfecting TRMT6 siRNA in HCT116 and RKO cells (n = 3). **F** Relative abundance of m1A methylated DIAPH3 mRNA in HCT116 and RKO cells after silencing TRMT6 (n = 3). **G** The relative expression of DIAPH3 mRNA in HCT116 and RKO cells after silencing TRMT6 siRNA (n = 3). *T6* TRMT6, *Neg* negative, *si si-RNA*, *CN* adjacent normal tissues, *CT* colorectal tumor, *RIP* RNA immunoprecipitation; **p < 0.01, *p < 0.05

transfection efficiency was validated by western blotting (Fig. 3A). Transwell assays were performed to examine the migration and invasion abilities, which were impaired in DIAPH3-depleted CRC cells (Fig. 3B–E). In addition, the wound healing assay indicated that silencing DIAPH3 attenuated the migration of CRC cells (Fig. 3F, G).

To further confirm the regulatory role of DIAPH3 in invasiveness, we knocked out DIAPH3 in HCT116 and RKO cells using the CRISPR/Cas9 system and validated its efficiency by genomic DNA sequencing (Fig. 4A) and western blotting (Fig. 4B). DIAPH3 knockout also significantly inhibited the migration and invasion of HCT116 and

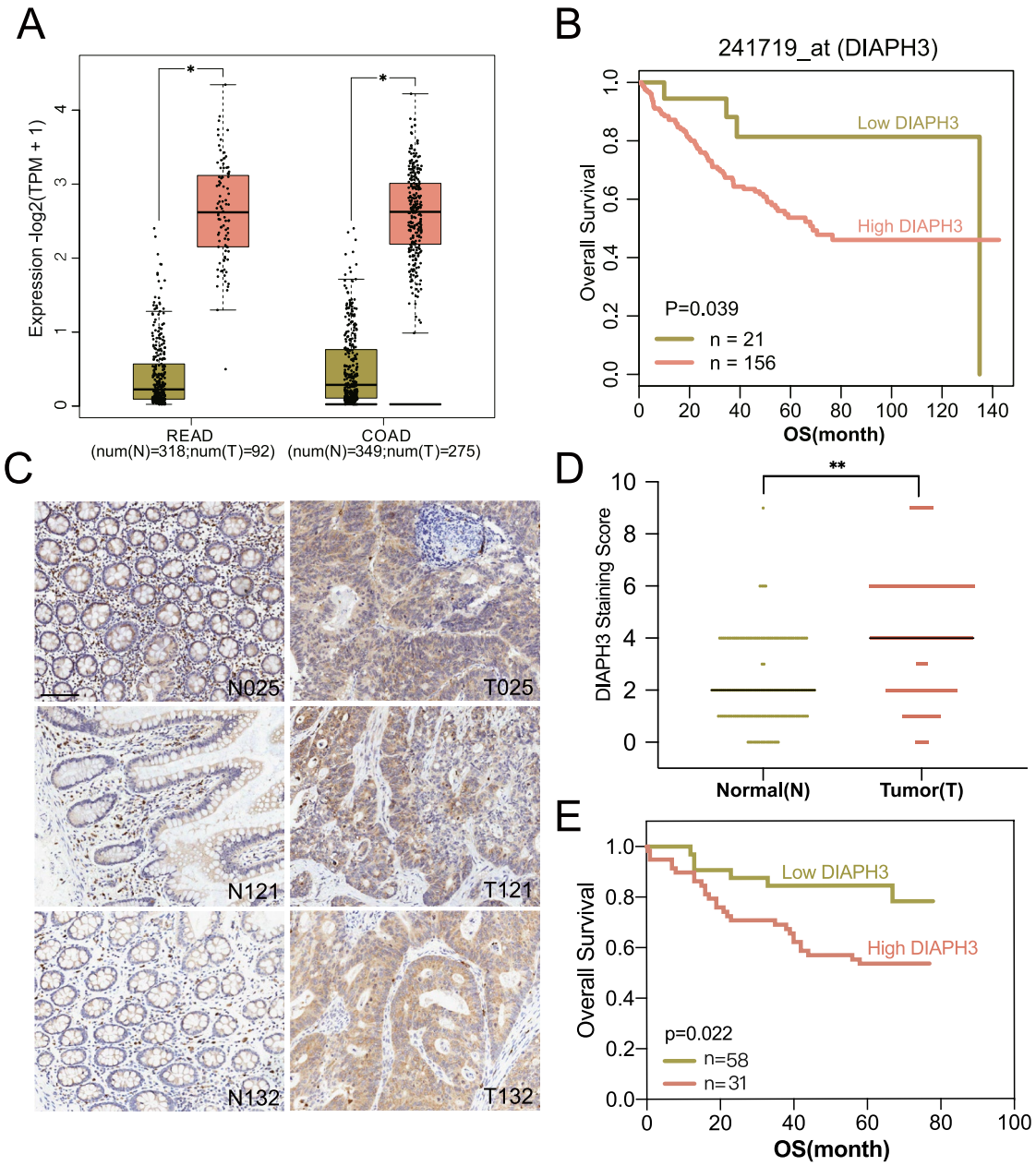

Fig. 2 The expression of DIAPH3 was upregulated in CRC. **A** The mRNA expression level of DIAPH3 in patients with rectum adenocarcinoma (READ) and colon adenocarcinoma (COAD) in the GEPIA database. Left (green): normal (N = 318 in READ, N = 349 in COAD); right (red): tumor (T = 92 in READ, T = 275 in COAD), error bars denote mean ± SEM. **B** Survival analysis based on the level of DIAPH3 expression in patients with CRC in GenomicScape database. **C** Representative images of DIAPH3 IHC staining in three pairs of CRC samples are shown (original magnification 200×). Scale bar, 100 μm. **D** IHC scores of DIAPH3 staining in matched CRC and normal tissues (n = 173). **E** Kaplan–Meier analysis of overall survival in CRC patients whose tumors display 'Low DIAPH3' versus 'High DIAPH3' expression. Log rank test, p = 0.022 (n = 89). *N* adjacent normal tissues, *T* CRC tissues, *READ* rectum adenocarcinoma, *COAD* colon adenocarcinoma, *OS* overall survival; **p < 0.01, *p < 0.05

RKO cells (Fig. 4C–F). Similarly, the wound healing assay indicated that DIAPH3 knockout attenuated the migration of CRC cells (Fig. 4G, H). In addition, to confirm the effect of DIAPH3 on CRC in vivo, negative-KO and DIAPH3-KO HCT116 cells were injected respectively into nude mice to establish a peritoneal metastasis model. In vivo luciferase bioluminescence imaging showed that luciferase signal intensity was significantly weaker in DIAPH3-KO HCT116 cells 35 days after peritoneal injection (Fig. 4I, J). The above in vivo and in vitro studies show that the invasiveness of CRC cells could be enhanced by DIAPH3.

Table 1 The correlation between the expression of DIAPH3 and the clinicopathological features in CRC

Clinical classification	DIAPH3 expression			
	Total number	Low (number)	High (number)	p Value
Gender				
Male	92	37	55	0.436
Female	84	29	55	
Age (years)				
≥ 65	91	34	57	0.969
< 65	85	32	53	
T stage				
T1/2	19	9	10	0.347
T3/4	157	57	100	
N stage				
N0	97	43	54	0.038
N1/2	79	23	56	
M stage				
M0	147	60	87	0.041
M1	29	6	23	
AJCC stage				
AJCC1/2	94	45	49	0.002
AJCC3/4	82	21	61	

AJCC American Joint Committee on Cancer, *N* lymph node, *M* metastasis, *T* tumor

KRT19 is a downstream target of DIAPH3

To investigate the underlying molecular mechanisms by which DIAPH3 regulates the invasion of CRC cells, we measured the protein spectrum using LC–MS/MS after silencing DIAPH3 in HCT116 cells, and proteins altered by over 1.3-fold were screened out (Fig. 5A). To further narrow the scope of potential downstream targets, we selected cancer-related genes that had been reported in previous studies and finally focused on seven potential targets, including four downregulated oncogenes and three upregulated tumor suppressors (Supplementary Table S4). This alteration was validated by western blotting in two CRC cell lines after knocking out DIAPH3, which showed that only KRT19 was consistently downregulated in both cell lines (Fig. 5B and Supplementary Fig. S5).

Previous study has reported that KRT19 plays a significant role in promoting colon cancer progression by upregulating Notch signaling [22]. To validate the role of KRT19 in the invasiveness of CRC cells, KRT19 was ectopically expressed in HCT116 and RKO cells (Fig. 5C). The role of KRT19 in the migration and invasion of CRC cells was examined using Transwell assays. KRT19-overexpressed CRC cells were seeded into uncoated or Matrigel-coated chambers. Crystal violet staining showed that more CRC cells overexpressing KRT19 passed through the micropores into the lower membrane (Fig. 5D–G). Based on these results, it is reasonable to suggest that DIAPH3, mRNA of which was modified by m1A modification, may play a role in colorectal cancer cell invasion and migration by influencing expression of the oncogene KRT19.

DIAPH3 regulated the invasiveness of CRC cells through KRT19

To determine whether KRT19 is indispensable for the invasiveness of CRC cells regulated by DIAPH3, we transfected a KRT19 ectopic overexpression plasmid into DIAPH3-deficient cells and validated the co-transfection efficiency by western blotting (Fig. 6A). Transwell assays showed that KRT19 overexpression rescued the decreased migration and invasion capabilities caused by DIAPH3 loss (Fig. 6B–E).

Although the protein level of KRT19 was significantly suppressed in DIAPH3-deficient CRC cells, the mRNA levels did not show consistent changes (Supplementary Fig. S6). In addition, there was no significant difference in KRT19 mRNA expression between tumor and normal tissues, as revealed by the GEPIA database (Supplementary Fig. S7). Therefore, we examined whether the DIAPH3-mediated downregulation of KRT19 involves post-transcriptional modifications. We first treated the cells with the protein biosynthesis inhibitor CHX to determine the stability of KRT19. Time-course analysis following the blockade of de novo protein synthesis indicated that DIAPH3 depletion shortened the half-life of endogenous KRT19 in HCT116 and RKO cells (Fig. 6F, G). Next, we treated cells with the proteasome inhibitor MG132 and the lysosome inhibitor 3-Methyladenine (3-MA). The results revealed that MG132

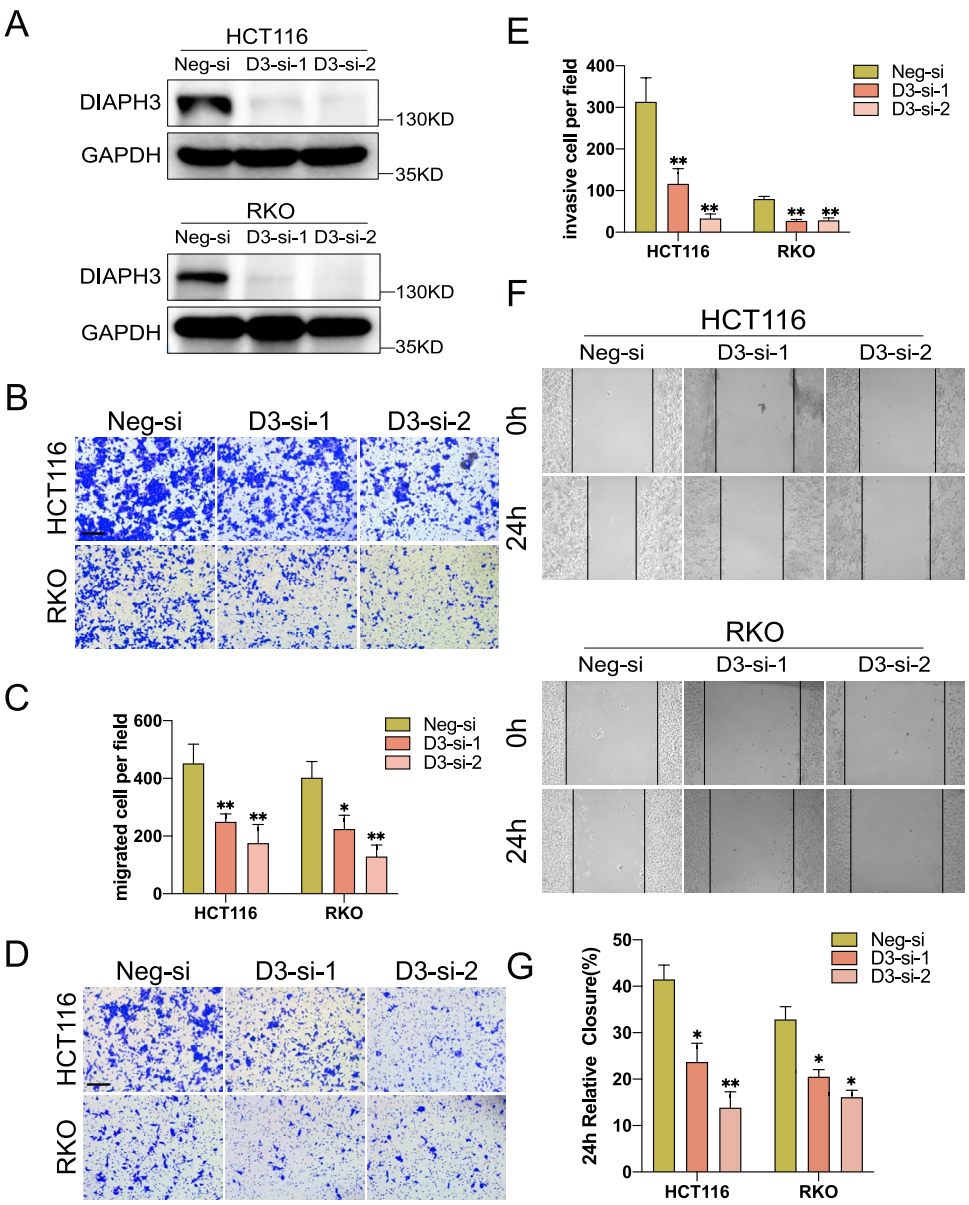

Fig. 3 DIAPH3 regulates the migration and invasion of human CRC cell lines. **A** The transfection efficiency of DIAPH3 siRNAs in HCT116 and RKO cells was validated by western blotting. **B** After seeding in the upper Transwell chamber and incubation for 48 h, HCT116 and RKO cells that migrated to the bottom of the membrane were stained with crystal violet. The representative images were captured under the microscope at a magnification of 200×. Scale bar, 200 μm. **C** The average number of migratory cells was counted in five random fields (n = 5). **D** After seeding in the Matrigel-coated chamber and incubation for 48 h, HCT116 and RKO cells that invaded the bottom of the membrane were stained with crystal violet. The representative images were captured under the microscope at a magnification of 200×. Scale bar, 200 μm. **E** The average number of invaded cells was counted in five random fields (n = 5). **F** Wound healing assays were conducted to compare the migration capabilities of CRC cells after knocking down DIAPH3 (n = 3). The difference in cell margin between 0 and 24 h showed moving track of cells. **G** Relative closure of the wound was quantified. D3, DIAPH3; Neg, Negative; si, siRNA; **p < 0.01; *p < 0.05

treatment significantly increased KRT19 protein expression in cells with DIAPH3 knockdown (Fig. 6H), whereas 3-MA treatment did not affect KRT19 protein levels (Supplementary Fig. S8). These results suggested that DIAPH3 regulates KRT19 degradation in a proteasome-dependent manner.

Discussion

More than 100 chemical modifications have been discovered in the transcriptome using high-throughput technologies [23]. Among these, m1A was recently discovered to play a regulatory role in mRNA expression [20]. m1A methylation occurs on a unique base that disrupts Watson–Crick base pairing and introduces a positive charge [24]. In tRNA and rRNA, m1A conserves tertiary structure and affects translation [25]. In mRNA, m1A mainly exists in the highly structured 5'-untranslated region near the start codon, indicating that it may affect the predicted secondary structure [26]. It has been reported that higher protein production was observed when a transcript carries the m1A modification around the initiation codon [5]. Additionally, m1A methylation affects the translation of the m1A-containing coding sequence in mitochondrial mRNA [27]. In this study, by applying m1A-seq, a method that relies on the immunoprecipitation of m1A-containing RNA fragments, we found that more genes with increased m1A methylation abundance showed upregulated mRNA expression levels, which is consistent with the findings of the above-mentioned studies.

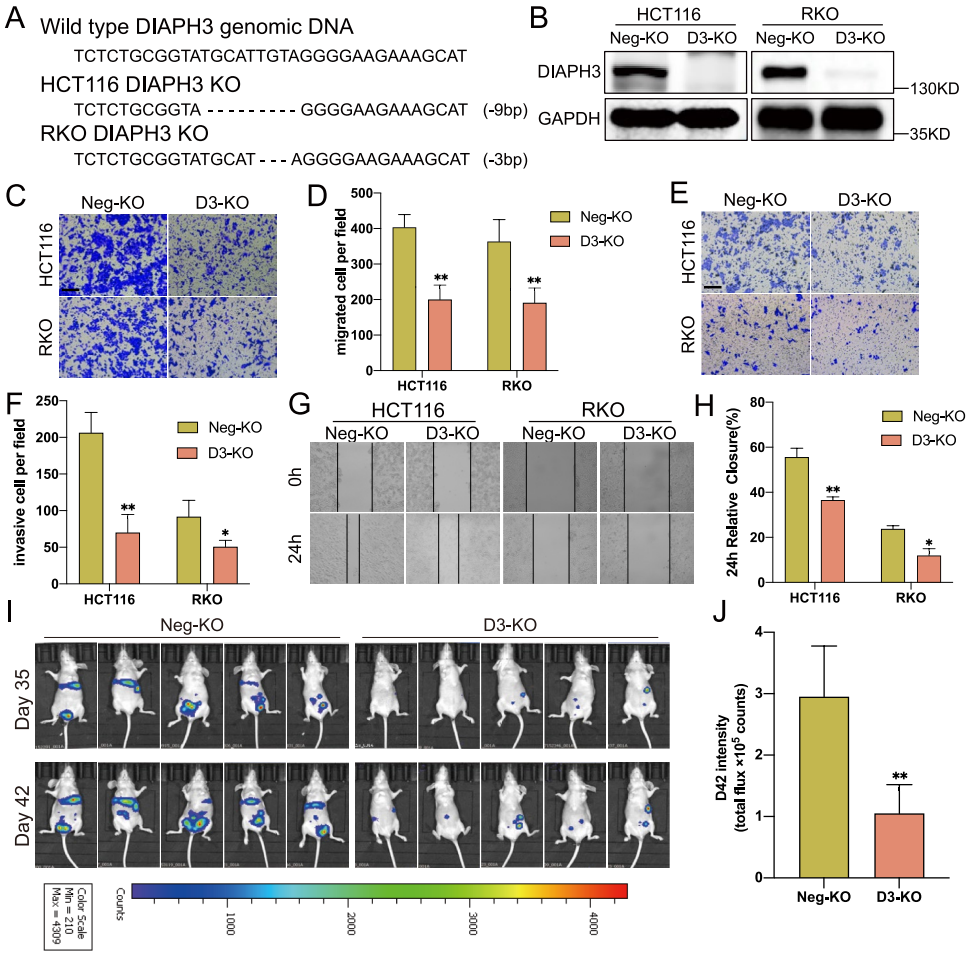

Fig. 4 Knocking out DIAPH3 inhibited the migration and invasion of CRC cells. **A** Genomic DNA sequences of DIAPH3 targeting site in HCT116 KO and RKO KO cell clones. **B** Knocking-out efficiency of DIAPH3 confirmed by western blotting. **C** After seeding in the upper Transwell chamber and incubation for 48 h, HCT116 and RKO cells that migrated to the bottom of the membrane were stained with crystal violet. The representative images were captured under the microscope at a magnification of 200×. Scale bar, 200 μm. **D** The average number of migratory cells was counted in five random fields (n = 5). **E** After seeding in the Matrigel-coated chamber and incubation for 48 h, HCT116 and RKO cells that invaded the bottom of the membrane were stained with crystal violet. The representative images were captured under the microscope at a magnification of 200×. Scale bar, 200 μm. **F** The average number of invaded cells was counted in five random fields (n = 5). **G** Wound healing assays were conducted to compare the migration capabilities of two CRC cells after knocking out DIAPH3 (n = 3). The difference in cell margin between 0 and 24 h showed moving track of cells. **H** Relative closure of the wound was quantified. **I** In vivo bioluminescence imaging of the mice injected with negative-KO and DIAPH3-KO HCT116 cells at the fifth and sixth week. **J** Quantitative analysis of bioluminescence imaging intensity on day 42 (n = 5). *D3* DIAPH3, *Neg* Negative, *KO* knock out; $^{**}p < 0.01$; $^{*}p < 0.05$

m1A regulators include methyltransferases, demethylases, and binding proteins that mediate m1A deposition, removal, and recognition. Dysregulated m1A regulators are associated with various cancers. By analyzing the data of CRC samples from TCGA, researchers have demonstrated that ALKBH3 and TRMT10C are correlated with good prognosis, ALKBH1 indicates poor prognosis, and TRMT61A and TRMT6 tend to correlate with poor prognosis [21]. In addition, one of the binding proteins of m1A—YTHDF1 was shown to regulate tumorigenicity and cancer stem cell-like activity in CRC [28]. However, the regulatory role of m1A methylation in CRC mRNA expression remains largely unknown. In this study, we confirmed that the expression of DIAPH3 was positively correlated with TRMT6, and that DIAPH3 mRNA expression levels were reduced after silencing the methyltransferase TRMT6, supporting DIAPH3 as an m1A-regulated gene.

As a member of the human formin family, DIAPH3 is involved in the polymerization of monomeric actin into linear filaments, and its dysregulation induces auditory alterations [29]. The role of DIAPH3 in cancer progression, especially metastasis, has been confirmed in many

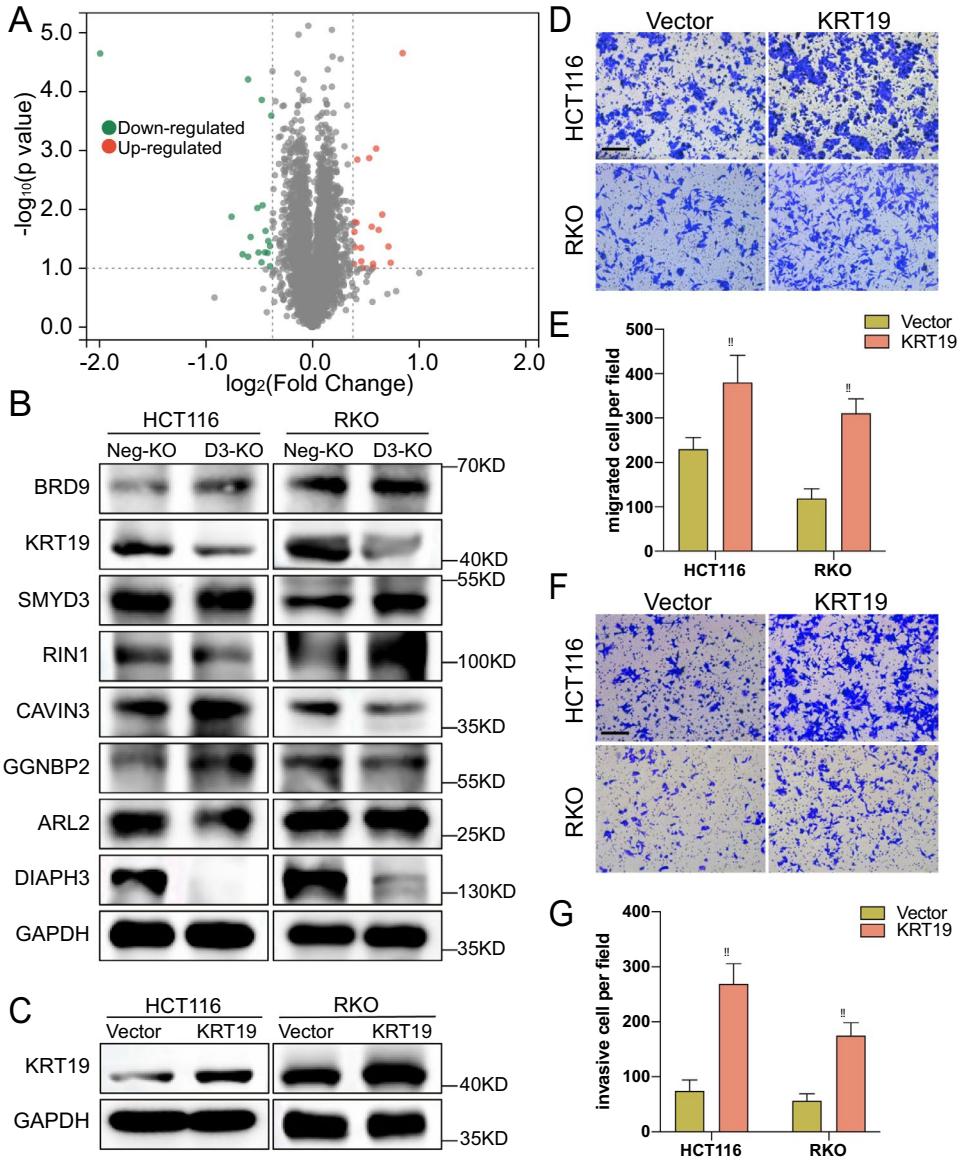

Fig. 5 Suppression of DIAPH3 induced the degradation of KRT19. **A** The Volcano Plots showed the distribution of genes with differential (up or down) expression after silencing DIAPH3 (n = 3). The fold change of expression of protein < 1.3 or p value > 0.1 is labeled as gray dots, while the others are marked with colorful dots. **B** Seven potential downstream targets of DIAPH3 were validated by western blotting after DIAPH3 was knocked out in HCT116 and RKO cells. **C** The HCT116 and RKO cells were transfected with KRT19 ectopic plasmids and the transfection efficiency was validated by western blotting. **D** After seeding in the upper Transwell chamber and incubation for 48 h, HCT116 and RKO cells that migrated to the bottom of the membrane were stained with crystal violet. The representative images were captured under the microscope at a magnification of 200×. Scale bar, 200 μm. **E** The average number of migratory cells was counted in five random fields (n = 5). **F** After seeding in the Matrigel-coated chamber and incubation for 48 h, HCT116 and RKO cells that invaded the bottom of the membrane were stained with crystal violet. The representative images were captured under the microscope at a magnification of 200×. Scale bar, 200 μm. **G** The average number of invaded cells was counted in five random fields (n = 5). *D3* DIAPH3, *Neg* negative, *KO* knock out; **p < 0.01

studies. For example, in breast cancer, DIAPH3 is crucial for the early stages of invadopodia formation and invasion of cancer cells [30]. DIAPH3 enhances the invasive ability of pancreatic cancer cells by activating selenoprotein TrxR1-mediated antioxidant effects [31]. Besides, it is also found that DIAPH3 is capable of promoting the metastasis of hepatocellular carcinoma by activating β/TCF signaling [32]. However, whether DIAPH3 plays a similar role in CRC has not been investigated. In the present study, we found that DIAPH3 was commonly upregulated in human CRC, probably due to its high m1A methylation level, and that DIAPH3 overexpression was related to poor survival and

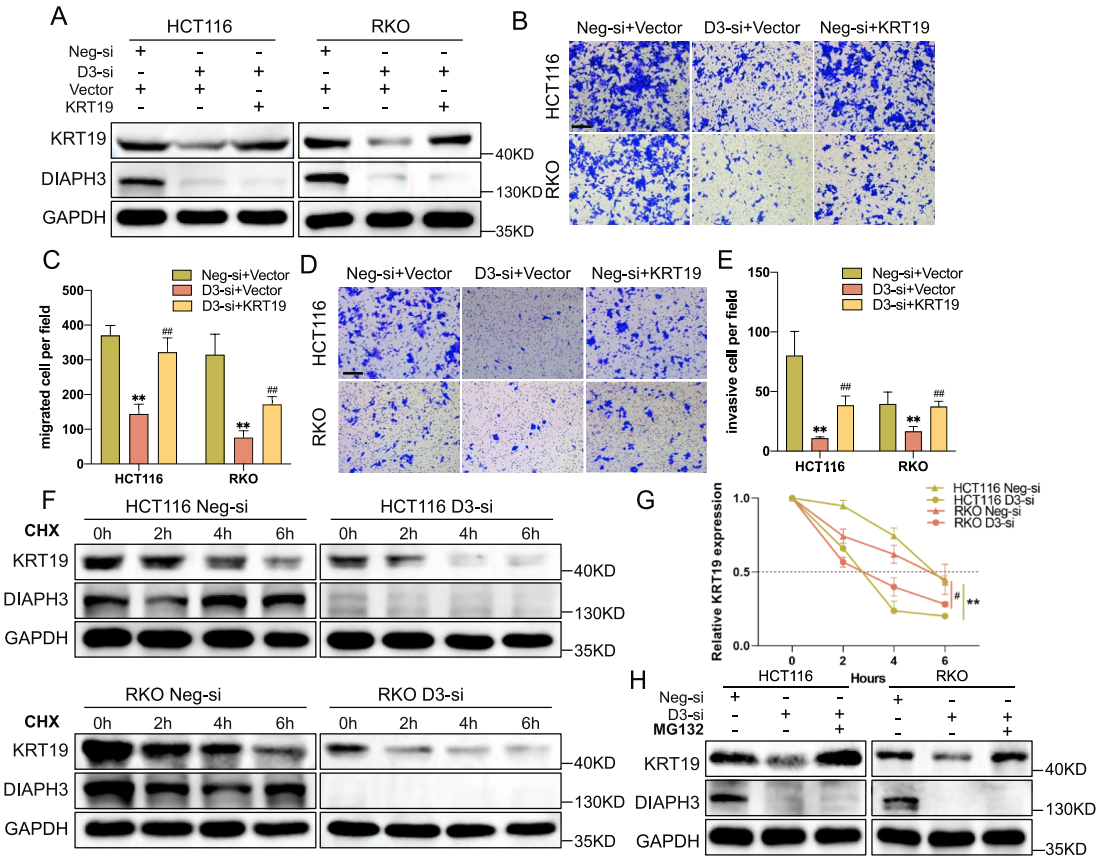

Fig. 6 DIAPH3 regulated the invasiveness of CRC cells through KRT19. **A** HCT116 and RKO cells were transfected with negative control siRNA or DIAPH3 siRNA, and then transfected with empty vector or KRT19 ectopic plasmid 48 h later. The transfection efficiency was assessed by western blotting. **B** After seeding in the upper Transwell chamber and incubation for 48 h, HCT116 and RKO cells that migrated to the bottom of the membrane were stained with crystal violet. The representative images were captured under the microscope at a magnification of 200×. Scale bar, 200 μm. **C** The average number of migratory cells was counted in five random fields (n = 5). $^{**}p < 0.01$ versus Neg si + Empty Vector; $^{\#\#}p < 0.01$ versus DIAPH3 si + Empty Vector. **D** After seeding in the Matrigel-coated chamber and incubation for 48 h, HCT116 and RKO cells that invaded the bottom of the membrane were stained with crystal violet. The representative images were captured under the microscope at a magnification of 200×. Scale bar, 200 μm. **E** The average number of invaded cells was counted in five random fields (n = 5). $^{**}p < 0.01$ versus Neg si + Empty Vector; $^{\#\#}p < 0.01$ versus DIAPH3 si + Empty Vector. **F** CRC cells with or without DIAPH3 silencing were treated with 100 mg/mL CHX and protein lysates were collected at indicated time points for western blot analysis. **G** KRT19 was quantified and plotted relative to the 0-time point. **H** MG132 (20 μM, 24 h) treatment on HCT116 and RKO cells with or without DIAPH3 silencing. $^{**}p < 0.01$, HCT116 DIAPH3-si versus HCT116 Negative-si group at the sixth hour; $^{\#}p < 0.05$, RKO DIAPH3-si versus RKO Negative-si group at the sixth hour. *D3* DIAPH3, *Neg* negative, *si* siRNA, *KO* knock out

distant metastasis. Moreover, we showed that CRC cells lacking DIAPH3 showed attenuated migratory and invasive capabilities and identified KRT19 as a potential downstream target of DIAPH3.

KRT19 is a type of intermediate filament that functions as a cytoskeletal scaffold in the nucleus and cytoplasm and plays potential roles in mechanical support and cell migration [33]. Interestingly, KRT19 had contradictory effects on tumorigenesis due to differential modulation of Wnt/β-catenin/notch signaling. On the one hand, KRT19 interacts with the β-catenin/RAC1 complex to suppress breast cancer progression through attenuation of Notch signaling. While, on the other hand, KRT19 directly interacts with β-catenin, promoting colon cancer progression by upregulating Notch signaling [22]. Moreover, KRT19 is correlated with cancer cell survival, invasion, and angiogenesis owing to its role in inhibiting senescence and E-cadherin expression [34]. In this study, we verified the pro-metastatic effect of KRT19 on CRC and found that the role of DIAPH3 in CRC metastasis is dependent on KRT19.

Furthermore, we elucidated the potential mechanism by which DIAPH3 mediated the degradation of KRT19. The ubiquitination-proteasome system and the autophagy-lysosome pathway are the two major degradation systems adopted by eukaryotic cells to regulate protein expression [35]. Generally, the autophagy inhibitor 3-MA and

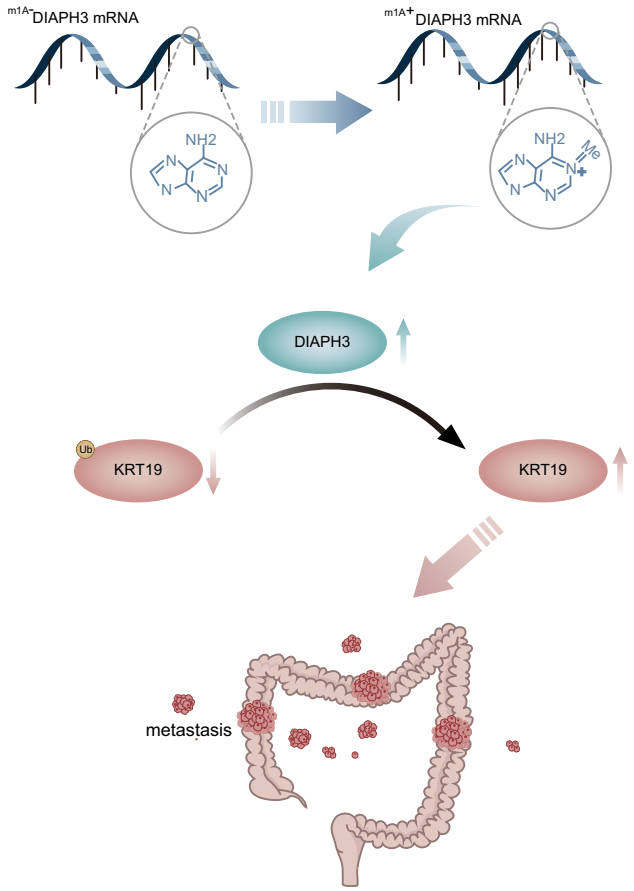

Fig. 7 Working model of DIAPH3 promoting CRC metastasis through KRT19. In CRC, m1A enhances the expression of DIAPH3 mRNA. Increased DIAPH3 suppresses the degradation of CLK3 in a proteasome-dependent manner, which accelerates CRC metastasis

proteasome inhibitor MG132 are used to identify how specific proteins are degraded [36]. Using inhibitors of these different degradation pathways, we observed that MG132 enhanced the KRT19 protein level in CRC cells lacking DIAPH3 expression, whereas 3-MA did not, indicating that DIAPH3 potentially plays its role through proteasome-dependent degradation of downstream KRT19 in CRC cells.

However, our study has some limitations. Firstly, the sample size for methylated RNA immunoprecipitation sequencing is not large enough and might bring bias. Secondly, the clear mechanisms through which m1A methylation regulates the mRNA expression of DIAPH3 requires further investigation. Recently, a newly published article reported that YTHDF1 is responsible for the recognition of the certain m1A methylated transcript, which could increase its stability [37]. Whether m1A modification can recruit a similar reader so that m1A influences the stability of the DIAPH3 transcript needs to be further explored.

Conclusion

Altogether, we found that DIAPH3 mRNA was modified and might upregulated in CRC cells through m1A methylation. Targeting DIAPH3 suppressed the migration and invasion of CRC cells, potentially through proteasome-dependent degradation of downstream KRT19 (Fig. 7), indicating that DIAPH3 is a promising therapeutic target for blocking metastasis in CRC.

Supplementary Information The online version contains supplementary material available at https://doi.org/10.1007/s10585-024-10323-0.

Author contributions Shuyi Mi and Jie Hu wrote the main manuscript text and Wenwen Chen and Jingyu Chen prepared Figs. 1–4. Zhipeng Xu and Meng Xue prepared Figs. 5–7. All authors reviewed the manuscript.

Funding The present study was supported by the Natural Science Foundation of Zhejiang Province （LMS25H160012）.

Data availability All data included in this study are available upon request by contact with the corresponding author. Data is provided within the supplementary information files.

Declarations

Conflict of interest The authors declare no competing interests.

Ethics approval Human ethics approval was obtained from the Human Research Ethics Committee of the Second Affiliated Hospital, School of Medicine, Zhejiang University. Informed consent was obtained from all the participants. Animal experiments were approved by the Animal Care and Use Committee of the Second Affiliated Hospital, School of Medicine, Zhejiang University.

Consent to participate All CRC patients provided informed consent for specimen collection before surgery.

References

1. Ushijima T, Clark SJ, Tan P (2021) Mapping genomic and epigenomic evolution in cancer ecosystems. Science 373(6562):1474–1479. https://doi.org/10.1126/science.abh1645

2. Porcellini E, Laprovitera N, Riefolo M, Ravaioli M, Garajova I, Ferracin M (2018) Epigenetic and epitranscriptomic changes in colorectal cancer: diagnostic, prognostic, and treatment implications. Cancer Lett 419:84–95. https://doi.org/10.1016/j.canlet.2018.01.049
3. He L, Li H, Wu A, Peng Y, Shu G, Yin G (2019) Functions of N6-methyladenosine and its role in cancer. Mol Cancer 18(1):176. https://doi.org/10.1186/s12943-019-1109-9
4. Garbo S, Zwergel C, Battistelli C (2021) m6A RNA methylation and beyond - the epigenetic machinery and potential treatment options. Drug Discov Today 26(11):2559–2574. https://doi.org/10.1016/j.drudis.2021.06.004
5. Dominissini D, Nachtergaele S, Moshitch-Moshkovitz S, Peer E, Kol N, Ben-Haim MS et al (2016) The dynamic N(1)-methyladenosine methylome in eukaryotic messenger RNA. Nature 530(7591):441–446. https://doi.org/10.1038/nature16998
6. Wu Y, Chen Z, Xie G, Zhang H, Wang Z, Zhou J et al (2022) RNA m(1)A methylation regulates glycolysis of cancer cells through modulating ATP5D. Proc Natl Acad Sci USA 119(28):e2119038119. https://doi.org/10.1073/pnas.2119038119
7. Su Z, Monshaugen I, Wilson B, Wang F, Klungland A, Ougland R et al (2022) TRMT6/61A-dependent base methylation of tRNA-derived fragments regulates gene-silencing activity and the unfolded protein response in bladder cancer. Nat Commun 13(1):2165. https://doi.org/10.1038/s41467-022-29790-8
8. Wang Y, Wang J, Li X, Xiong X, Wang J, Zhou Z et al (2021) N(1)-methyladenosine methylation in tRNA drives liver tumourigenesis by regulating cholesterol metabolism. Nat Commun 12(1):6314. https://doi.org/10.1038/s41467-021-26718-6
9. Sung H, Ferlay J, Siegel RL, Laversanne M, Soerjomataram I, Jemal A et al (2021) Global cancer statistics 2020: GLOBOCAN estimates of incidence and mortality worldwide for 36 cancers in 185 countries. CA Cancer J Clin 71(3):209–249. https://doi.org/10.3322/caac.21660
10. Brouwer NPM, Bos A, Lemmens V, Tanis PJ, Hugen N, Nagtegaal ID et al (2018) An overview of 25 years of incidence, treatment and outcome of colorectal cancer patients. Int J Cancer 143(11):2758–2766. https://doi.org/10.1002/ijc.31785
11. Shi L, Chen W, Zhang Z, Chen J, Xue M (2021) N1-methyladenosine profiling of long non-coding RNA in colorectal cancer. IUBMB Life 73(10):1235–1243. https://doi.org/10.1002/iub.2534
12. Chen W, Wang H, Mi S, Shao L, Xu Z, Xue M (2023) ALKBH1-mediated m(1) A demethylation of METTL3 mRNA promotes the metastasis of colorectal cancer by downregulating SMAD7 expression. Mol Oncol 17(2):344–364. https://doi.org/10.1002/1878-0261.13366
13. Xue M, Mi S, Zhang Z, Wang H, Chen W, Wei W et al (2023) MFAP2, upregulated by m1A methylation, promotes colorectal cancer invasiveness via CLK3. Cancer Med 12(7):8403–8414. https://doi.org/10.1002/cam4.5561
14. Smith JJ, Deane NG, Wu F, Merchant NB, Zhang B, Jiang A et al (2010) Experimentally derived metastasis gene expression profile predicts recurrence and death in patients with colon cancer. Gastroenterology 138(3):958–968. https://doi.org/10.1053/j.gastro.2009.11.005
15. Martin MJ (2011) Cutadapt removes adapter sequences from high-throughput sequencing reads. EMBnet 17:10–12
16. Kim D, Paggi JM, Park C, Bennett C, Salzberg SL (2019) Graph-based genome alignment and genotyping with HISAT2 and HISAT-genotype. Nat Biotechnol 37(8):907–915. https://doi.org/10.1038/s41587-019-0201-4
17. Zhang Y, Liu T, Meyer CA, Eeckhoute J, Johnson DS, Bernstein BE et al (2008) Model-based analysis of ChIP-Seq (MACS). Genome Biol 9(9):R137. https://doi.org/10.1186/gb-2008-9-9-r137
18. Shen L, Shao NY, Liu X, Maze I, Feng J, Nestler EJ (2013) diffReps: detecting differential chromatin modification sites from ChIP-seq data with biological replicates. PLoS ONE 8(6):e65598. https://doi.org/10.1371/journal.pone.0065598
19. Trapnell C, Williams BA, Pertea G, Mortazavi A, Kwan G, van Baren MJ et al (2010) Transcript assembly and quantification by RNA-Seq reveals unannotated transcripts and isoform switching during cell differentiation. Nat Biotechnol 28(5):511–515. https://doi.org/10.1038/nbt.1621
20. Zhao BS, Roundtree IA, He C (2017) Post-transcriptional gene regulation by mRNA modifications. Nat Rev Mol Cell Biol 18(1):31–42. https://doi.org/10.1038/nrm.2016.132
21. Zhao Y, Zhao Q, Kaboli PJ, Shen J, Li M, Wu X et al (2019) m1A regulated genes modulate PI3K/AKT/mTOR and ErbB pathways in gastrointestinal cancer. Transl Oncol 12(10):1323–1333. https://doi.org/10.1016/j.tranon.2019.06.007
22. Saha SK, Yin Y, Chae HS, Cho SG (2019) Opposing regulation of cancer properties via KRT19-mediated differential modulation of Wnt/beta-Catenin/Notch signaling in breast and colon cancers. Cancers. https://doi.org/10.3390/cancers11010099
23. Boccaletto P, Stefaniak F, Ray A, Cappannini A, Mukherjee S, Purta E et al (2022) MODOMICS: a database of RNA modification pathways. 2021 update. Nucleic Acids Res 50(D1):D231–D235. https://doi.org/10.1093/nar/gkab1083
24. Zhou H, Kimsey IJ, Nikolova EN, Sathyamoorthy B, Grazioli G, McSally J et al (2016) m(1)A and m(1)G disrupt A-RNA structure through the intrinsic instability of Hoogsteen base pairs. Nat Struct Mol Biol 23(9):803–810. https://doi.org/10.1038/nsmb.3270
25. Xiong X, Li X, Yi C (2018) N(1)-methyladenosine methylome in messenger RNA and non-coding RNA. Curr Opin Chem Biol 45:179–186. https://doi.org/10.1016/j.cbpa.2018.06.017
26. Zhang LS, Liu C, Ma H, Dai Q, Sun HL, Luo G et al (2019) Transcriptome-wide mapping of internal N(7)-methylguanosine methylome in mammalian mRNA. Mol Cell 74(6):1304–1316. https://doi.org/10.1016/j.molcel.2019.03.036
27. Machnicka MA, Milanowska K, Osman Oglou O, Purta E, Kurkowska M, Olchowik A et al (2013) MODOMICS: a database of RNA modification pathways–2013 update. Nucleic Acids Res. 41:D262-267. https://doi.org/10.1093/nar/gks1007
28. Bai Y, Yang C, Wu R, Huang L, Song S, Li W et al (2019) YTHDF1 regulates tumorigenicity and cancer stem cell-like activity in human colorectal carcinoma. Front Oncol 9:332. https://doi.org/10.3389/fonc.2019.00332
29. Labat-de-Hoz L, Alonso MA (2021) Formins in human disease. Cells. https://doi.org/10.3390/cells10102554
30. Lizarraga F, Poincloux R, Romao M, Montagnac G, Le Dez G, Bonne I et al (2009) Diaphanous-related formins are required for invadopodia formation and invasion of breast tumor cells. Cancer Res 69(7):2792–2800. https://doi.org/10.1158/0008-5472.CAN-08-3709
31. Rong Y, Gao J, Kuang T, Chen J, Li JA, Huang Y et al (2021) DIAPH3 promotes pancreatic cancer progression by activating selenoprotein TrxR1-mediated antioxidant effects. J Cell Mol Med 25(4):2163–2175. https://doi.org/10.1111/jcmm.16196
32. Dong L, Li Z, Xue L, Li G, Zhang C, Cai Z et al (2018) DIAPH3 promoted the growth, migration and metastasis of hepatocellular carcinoma cells by activating beta-catenin/TCF signaling. Mol Cell Biochem 438(1–2):183–190. https://doi.org/10.1007/s11010-017-3125-7
33. Coulombe PA, Wong P (2004) Cytoplasmic intermediate filaments revealed as dynamic and multipurpose scaffolds. Nat Cell Biol 6(8):699–706. https://doi.org/10.1038/ncb0804-699

34. Takano M, Shimada K, Fujii T, Morita K, Takeda M, Nakajima Y et al (2016) Keratin 19 as a key molecule in progression of human hepatocellular carcinomas through invasion and angiogenesis. BMC Cancer 16(1):903. https://doi.org/10.1186/s12885-016-2949-y
35. McShane E, Selbach M (2022) Physiological functions of intracellular protein degradation. Annu Rev Cell Dev Biol 38:241–262. https://doi.org/10.1146/annurev-cellbio-120420-091943
36. Wu X, Zheng Y, Liu M, Li Y, Ma S, Tang W et al (2021) BNIP3L/NIX degradation leads to mitophagy deficiency in ischemic brains. Autophagy 17(8):1934–1946. https://doi.org/10.1080/15548627.2020.1802089
37. Gu X, Zhuang A, Yu J, Yang L, Ge S, Ruan J et al (2024) Histone lactylation-boosted ALKBH3 potentiates tumor progression and diminished promyelocytic leukemia protein nuclear condensates by m1A demethylation of SP100A. Nucleic Acids Res 52(5):2273–2289. https://doi.org/10.1093/nar/gkad1193